Nonequilibrium dynamics of a stochastic model of anomalous heat transport: numerical analysis

2010 J. Phys. A: Math. Theor. 43 145001

(http://iopscience.iop.org/1751-8121/43/14/145001)

IOP PUBLISHING JOURNAL OF PHYSICS A: MATHEMATICAL AND THEORETICAL

J. Phys. A: Math. Theor. **43** (2010) 145001 (16pp) doi:10.1088/1751-8113/43/14/145001

Nonequilibrium dynamics of a stochastic model of anomalous heat transport: numerical analysis

L Delfini[1,4], S Lepri[1], R Livi[2,3], C Mejía-Monasterio[1,5] and A Politi[1]

[1] Istituto dei Sistemi Complessi, Consiglio Nazionale delle Ricerche, via Madonna del Piano 10, I-50019 Sesto Fiorentino, Italy
[2] Dipartimento di Fisica, Università di Firenze, via G. Sansone 1 I-50019, Sesto Fiorentino, Italy
[3] Sezione INFN, and CSDC Firenze, via G. Sansone 1 I-50019, Sesto Fiorentino, Italy

E-mail: antonio.politi@isc.cnr.it

Received 9 November 2009, in final form 17 February 2010
Published 16 March 2010
Online at stacks.iop.org/JPhysA/43/145001

Abstract

We study heat transport in a chain of harmonic oscillators with random elastic collisions between nearest-neighbours. The equations of motion of the covariance matrix are numerically solved for free and fixed boundary conditions. In the thermodynamic limit, the shape of the temperature profile and the value of the stationary heat flux depend on the choice of boundary conditions. For free boundary conditions, they also depend on the coupling strength with the heat baths. Moreover, we find a strong violation of local equilibrium at the chain edges that determine two boundary layers of size $\sqrt{N}$ (where N is the chain length) that are characterized by a different scaling behaviour from the bulk. Finally, we investigate the relaxation towards the stationary state, finding two long time scales: the first corresponds to the relaxation of the hydrodynamic modes; the second is a manifestation of the finiteness of the system.

PACS numbers: 05.60.-k, 05.70.Ln, 44.10.+i

(Some figures in this article are in colour only in the electronic version)

1. Introduction

The problem of heat transport in chains of oscillators is one of the most relevant testing grounds to understand the behaviour of statistical systems steadily kept out of equilibrium. In the last decade, numerical simulations and analytic arguments have contributed to clarify the behaviour of such systems in the thermodynamic limit (see review papers [1–3] and references therein).

[4] Present address: Laboratoire de Physique Théorique (IRSAMC), Université de Toulouse (CNRS-UPS), F-31062 Toulouse, France.
[5] Present address: University of Helsinki, Department of Mathematics and Statistics, PO Box 68 FIN-00014, Helsinki, Finland.

With the advent of nanoscopics, the importance of this physical setup is further strengthened by the possibility of comparing theoretical predictions with the experimental results on e.g. the heat conduction properties of individual nanotubes [4]. However, there is still a number of open questions such as the role of boundary conditions (BC in the following) and the convergence towards the stationary state. In spite of the continuous increase in computer performances, direct numerical simulations are still not so effective as to provide reliable data on sufficiently large systems. In this respect, stochastic models like the one introduced in [5] are proved to be very helpful. In this paper we consider a version of such models already analysed in [6, 7]. The model consists in a chain of N coupled harmonic oscillators in interaction (at the boundaries) with two stochastic heat baths at different temperatures. In addition, the oscillators are subject to stochastic collisions that exchange the momenta of randomly chosen pairs of neighbouring oscillators, so that both energy and momentum are conserved. In a sense, collisions simulate the presence of nonlinear terms, as they contribute to ensuring ergodicity of an otherwise integrable model. On a quantitative level, it is not clear whether models such as the FPU-β chain are characterized by the same divergence rate of the heat conductivity. However, the shape of the temperature profile in the stochastic model is almost identical to that for the FPU system [6], and strong similarities are also found when comparing other two-point correlators. Moreover, since the collision rule yields a linear process, the evolution equations for ensemble averages can be written in exact form and thereby solved numerically, without having to deal with the statistical fluctuations that affect finite samples. As a result, we have found that the invariant measure can be effectively approximated by the product of Gaussian distributions aligned along the eigendirections of the covariance matrix [6]. Moreover, in [7], we investigated the continuum limit (which corresponds to the large-N limit) of the covariance matrix, deriving suitable partial differential equations for the stationary state, in the case of fixed BC. As a result, we have obtained explicit formulae for the temperature profile and the energy current. Remarkably, this is the first example of an analytic expression for the temperature profile in a system characterized by anomalous heat transport.

In [8] we go beyond, by extending the continuum limit to include the time dependence of the covariance matrix. The reader is thus referred to [8] for a more detailed introduction and the corresponding bibliography. The aim of this paper is to complement the analysis contained in [8] with accurate numerical studies of finite samples with the goal of clarifying those issues that are too difficult to be worked out analytically. We start by numerically computing the stationary covariance for both free and fixed BC. This helps to shed some light on the nontrivial role played by BC, whenever heat transport exhibits an anomalous behaviour. In the presence of normal transport, one expects that BC affect only a finite boundary layer so that, in the thermodynamic limit, the leading term of the heat flux is independent of BC. On the other hand, it is known that in disordered chains of linear oscillators, the same system may even behave as a thermal superconductor or as an insulator, by simply switching from free to fixed BC [9]. In generic nonlinear chains, numerical simulations suggest that the heat flux scales in the same way, independently of BC. However, the careful simulations performed in [10] revealed that in the FPU-β model, the ratio between the heat fluxes measured for free and fixed BC does not converge to 1 for $N \to \infty$. Here we show that the same behaviour occurs in our stochastic model. Actually the dependence on BC is even more subtle than one could have imagined: while in the case of fixed BC, the heat flux and the temperature profile are asymptotically independent of the coupling strength with the thermal baths, the same is not true for free BC.

A second objective of this paper is the analysis of the convergence towards the steady state. This question, which has been hardly discussed in the literature, can be straightforwardly addressed for our model, as it amounts to computing the eigenvalues of the evolution operator

for the covariances. Moreover, we also compare the convergence of the average heat flux for different system sizes to show how careful direct simulations must be, if they have to be trusted. We find that finite-size effects associated with the relaxation rates of slow, i.e. long-wavelength, modes significantly modify the asymptotic scaling of the relaxation process. In practice, we find numerical evidence that the theoretical hydrodynamic scaling holds only over a finite range of time scales, although its duration diverges with N.

The paper is organized as follows. In section 2, we briefly recall the definition of the covariance matrix, and the coupled equations governing its evolution towards the stationary value. Some properties of the steady state are discussed in section 3. The problem of the approach to the steady state is addressed in section 4. Finally, in section 5 we summarize our main results.

2. Equations for the covariance matrix

In this section, we introduce the minimal notations and definitions needed to follow the main discussion presented in the following sections. The reader interested in a more detailed presentation is referred to [8]. We consider a chain of N unit-mass particles interacting via nearest-neighbour harmonic coupling of the frequency ω. The equations of motion are given by

$$\begin{aligned} \dot{q}_n &= p_n \\ \dot{p}_n &= \omega^2(q_{n+1} - 2q_n + q_{n-1}) + \delta_{n,1}(\xi^+ - \lambda\dot{q}_1) + \delta_{n,N}(\xi^- - \lambda\dot{q}_N), \end{aligned} \tag{1}$$

where p_n and q_n are the momentum and displacement from the equilibrium position of the nth particle respectively, $\delta_{i,j}$ is the Kronecker delta and $\xi^\pm$ are independent Wiener processes with zero mean and variance $2\lambda k_B T_\pm$, where k_B is the Boltzmann constant and λ is the coupling constant (also known as white noise). In addition, the deterministic dynamics is perturbed by random binary collisions in which nearest-neighbour oscillators exchange their momenta, and occurring at a rate γ. Therefore, in these collisions the total momentum and energy are conserved. In the following, free and fixed boundary conditions will be considered. These can be expressed in terms of the position variable q as $q_0 = q_1$, $q_N = q_{N+1}$ for *free* BC and $q_0 = q_{N+1} = 0$ for *fixed* BC.

We consider the covariance matrix written as

$$\mathbf{c} = \begin{pmatrix} \mathbf{y} & \mathbf{z} \\ \mathbf{z}^\dagger & \mathbf{v} \end{pmatrix}, \tag{2}$$

where the matrices $\mathbf{y}$, $\mathbf{z}$ and $\mathbf{v}$ of respective dimensions $(N-1)\times(N-1)$, $(N-1)\times N$ and $N\times N$ are defined as

$$\mathbf{y}_{i,j} = \langle \Delta q_i \Delta q_j \rangle, \qquad \mathbf{z}_{i,j} = \langle \Delta q_i p_j \rangle, \qquad \mathbf{v}_{i,j} = \langle p_i p_j \rangle, \tag{3}$$

where $\langle\cdot\rangle$ denotes the average over phase space probability distribution function P and $\Delta q_i = q_i - q_{i-1}$ stand for the particle relative displacements. The variables $(\Delta q_i, p_i)$ are the convenient choice to deal with: on the one hand, absolute positions are not well defined for free BC and on the other hand, the potential energy is expressed in terms of relative differences. The only subtlety is that the domain of definition of Δq_i differs from that of p_i. Thereby, the bulk of the system is defined as $\{\Delta q_i \mid i \in [2, N]\}$ and $\{p_i \mid i \in [2, N-1]\}$. The evolution equations for $\mathbf{c}$ in the bulk are

$$\begin{aligned} \dot{\mathbf{y}}_{i,j} &= \mathbf{z}_{j,i} - \mathbf{z}_{j,i-1} + \mathbf{z}_{i,j} - \mathbf{z}_{i,j-1}, \\ \dot{\mathbf{z}}_{i,j} &= \mathbf{v}_{i,j} - \mathbf{v}_{i-1,j} + \omega^2(\mathbf{y}_{i,j+1} - \mathbf{y}_{i,j}) + \gamma(\mathbf{z}_{i,j+1} + \mathbf{z}_{i,j-1} - 2\mathbf{z}_{i,j}), \\ \dot{\mathbf{v}}_{i,j} &= \omega^2(\mathbf{z}_{j+1,i} - \mathbf{z}_{j,i} + \mathbf{z}_{i+1,j} - \mathbf{z}_{i,j}) + \gamma\mathbf{W}_{i,j}. \end{aligned} \tag{4}$$

These equations follow from the deterministic equations of motion (1) plus the contribution of the stochastic noise (γ denotes the collision rate), that is described by the collision matrix $\mathbf{W}$,

$$\mathbf{W}_{ij} \equiv \begin{cases} \mathbf{v}_{i-1,j-1} + \mathbf{v}_{i+1,j+1} - 2\mathbf{v}_{i,j} & i = j \\ \mathbf{v}_{i-1,j} + \mathbf{v}_{i,j+1} - 2\mathbf{v}_{i,j} & i - j = -1 \\ \mathbf{v}_{i+1,j} + \mathbf{v}_{i,j-1} - 2\mathbf{v}_{i,j} & i - j = 1 \\ \mathbf{v}_{i+1,j} + \mathbf{v}_{i-1,j} + \mathbf{v}_{i,j-1} + \mathbf{v}_{i,j+1} - 4\mathbf{v}_{i,j} & |i - j| > 1 \end{cases}. \tag{5}$$

On the boundaries, several changes appear in the velocity fields. The interested reader can find a full description in section 2.2 of [8]. Here we limit ourselves to show the contribution arising from the coupling with the heat bath, namely

$$\mathbf{z}^b_{i,j} = \delta_{j,1}\mathbf{z}_{i,1} + \delta_{j,N}\mathbf{z}_{i,N},$$

$$\mathbf{v}^b_{i,j} = \delta_{j,1}\mathbf{v}_{i,1} + \delta_{j,N}\mathbf{v}_{i,N} + \delta_{i,1}\mathbf{v}_{1,j} + \delta_{i,N}\mathbf{v}_{N,j} - 2\lambda k_B(T_+\delta_{i,1}\delta_{j,1} + T_-\delta_{i,N}\delta_{j,N}).$$

3. Stationary covariance

In this section we investigate some properties of the nonequilibrium steady state, for both fixed and free BC. The stationary state is obtained by considering the time-independent solution of equations (4). It can be efficiently determined by exploiting the sparsity of the corresponding linear problem, as well as the symmetries of the unknowns (this approach has been followed in [6] for fixed BC). Alternatively, one can just let evolve equations (4) starting from any meaningful initial conditions, as the dynamics will necessarily converge towards the only stable stationary state (here we have adopted this latter approach also because we wish to study the convergence—see in the following). The integration of equation (4) has been performed by means of a standard fourth-order Runge–Kutta algorithm and using a time step $\delta t = 0.01$. All numerical results presented in this paper have been obtained for $\omega = 1, T_+ = 1.5, T_- = 0.5$. This is by no means a limitation, as all these parameters can be easily scaled out due to the linear structure of the model. Accordingly, they will not be mentioned again, unless specifically needed for a comparison with theoretical predictions.

3.1. The heat flux

The first observable we have looked at is the energy flux at the position i which, in terms of the matrices $\mathbf{v}$, $\mathbf{z}$, is written as [9]

$$J_i = -\omega^2 \mathbf{z}_{i+1,i+1} + \frac{\gamma}{2}(\mathbf{v}_{i,i} - \mathbf{v}_{i+1,i+1}). \tag{6}$$

We have adopted the convention that a positive flux corresponds to a propagation towards increasing values of the spatial index i. The first term stems from the deterministic forces that, according to the scalings predicted in [8], are responsible for the leading (anomalous) contribution[6]. The second term accounts for energy exchanges due to collisions of nearby particles. In the stationary state, J_i is independent of i, i.e. $J_i \equiv J$.

In figure 1, we show $J\sqrt{N}$ as a function of the inverse of the system size N. The results refer to free BC (as we do not have analytic estimates to compare with), $\lambda = 1$ and different values of the collision rate γ (see the various symbols as described in the figure caption). In all cases there is convincing evidence that $J \sim N^{-1/2}$, similar to what predicted analytically in

[6] In the literature, seemingly different definitions of the heat flux may be found. The difference typically relies in the addition of irrelevant (zero average) time derivatives of terms such as $q_i q_{i+1}$.

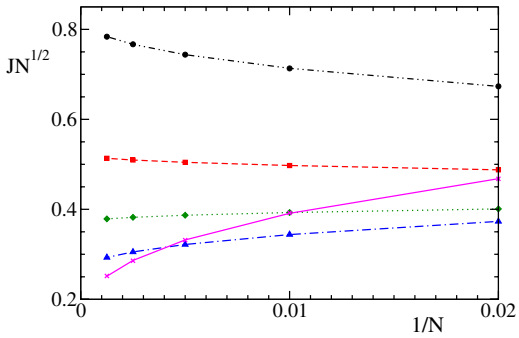

Figure 1. Free BC ($\lambda = 1$): the scaled stationary flux $J\sqrt{N}$ versus $1/N$ for $\gamma = 0.2$ (circles), 0.5 (squares), 1 (diamonds), 2 (triangles), 5 (crosses). The lines are obtained by fitting the data with equation (7).

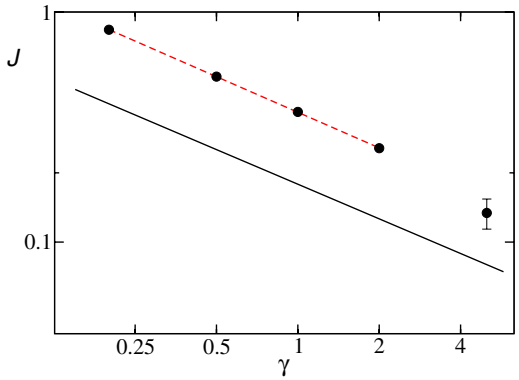

Figure 2. Asymptotic value of $\mathcal{J}$ as a function of the collision rate γ for free BC and the same parameter values as in figure 1. Data are plotted in log–log scales. The error bar for $\gamma = 5$ has been estimated from a rough comparison among different extrapolation schemes. The dashed line is a power law fit of the first four data: its slope is -0.51. The solid line corresponds to the analytic solution for fixed BC (equation (20) of [7]).

[7] for the case of fixed BC. As a consequence, the effective conductivity, $\kappa \equiv JN/(T_+ - T_-)$, diverges as $\sqrt{N}$. However, from figure 1 the presence of sub-leading singular corrections which hinder the extrapolation of the asymptotic value is also evident . In analogy with [7], we introduce the ansatz

$$J = \frac{\mathcal{J}}{\sqrt{N}} + \frac{B}{N^{\beta}}. \tag{7}$$

By using this formula to fit the data, we obtain the curves reported in figure 1 which reproduce quite well the raw data. Note that the convergence is from below for smaller γ values, while from above for larger collision rates. All the estimated β values range in the interval [0.88, 0.95], suggesting that this parameter may be 'universal'.

The extrapolated $\mathcal{J}$ values are plotted in figure 2, where we can see that $\mathcal{J} \sim \gamma^{-1/2}$, as found for fixed BC [7] . For $\gamma = 5$, the extrapolated value of $\mathcal{J}$ suffers a substantial uncertainty due to large finite-size corrections (that become even more sizeable for yet larger γ values).

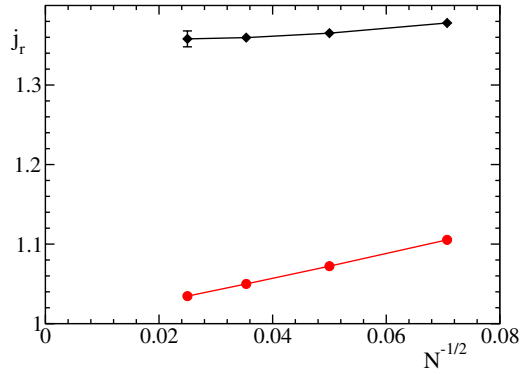

Figure 3. Ratio of the energy fluxes as defined in equation (8), for free (diamonds) and fixed (circles) BC as a function of $1/\sqrt{N}$, and for $\gamma = 1$. The error on j_r for free BC and $N = 1600$ is due to a not yet relaxed dynamics.

So far, we have not found any relevant difference between fixed and free BC. The heat flux scales in the same way in both cases and exhibits the same dependence on the collision rate. If the effect of the BC were restricted to a layer of finite width around the boundary, in the thermodynamic limit, the thermal resistance of a given chain would be independent of the type of thermal contact. In other words, we should expect $\mathcal{J}$ to be independent of the BC. However, this is not the case, as can be inferred from figure 2, where we have also plotted the analytic curve for the fixed BC case (equation (20) in [7]). For free BC, the heat flux is approximately twice as that obtained for fixed BC. It is worth mentioning that the same effect was found in the simulations of FPU-β chains [10], although with a slightly different value of the ratio (around 1.7 in that case). Since the flux is constant along the chain, this means that even deeply in the bulk, the system perceives the effect of the boundaries. In particular, from the knowledge of the local temperature profile and from the heat flux, one can in principle infer the type of BC. These results suggest that this is another way in which anomalous conduction manifests itself.

The whole scenario is even more subtle than suggested in figure 2. In fact, for free BC, the leading term of the heat flux depends not only on γ but also on the coupling strength λ with the heat bath, while this is not so for fixed BC. We illustrate this in figure 3, where we plot the ratio

$$j_r = j(\lambda = 1, N)/j(\lambda = 1/4, N) \tag{8}$$

where $j(\lambda, N)$ is the heat flux in a chain of length N and for a given value of λ. It is not surprising to see that the coupling with the heat baths modifies the flux in chains of finite length. However, we see that for fixed BC, the effect of the coupling vanishes as j_r converges to 1 (see the lower curve in figure 3). In contrast, for free BC, j_r remains significantly different from 1. This suggests that fixed BC may lead to a kind of universal behaviour, namely the heat flux and the temperature profile are independent of the details of the coupling with the heat baths. This is not the case for free BC. It would be interesting to check whether the same holds true in generic nonlinear chains.

3.2. The temperature profile

Another observable of interest is the temperature profile $T_i = \langle p_i^2 \rangle$. In figure 4 we show the temperature profile for free BC and three different sizes, as a function of the 'normalized'

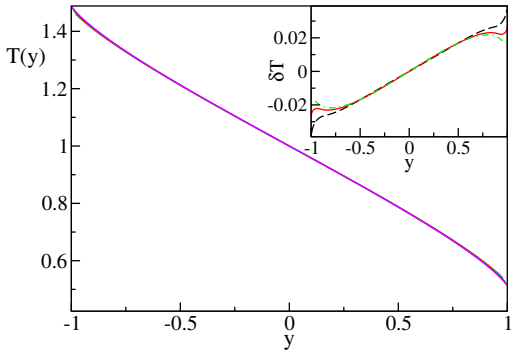

Figure 4. Temperature profile $T(y)$ for $\gamma = 1$ and $\lambda = 1$ and free BC, for $N = 100, 200, 400$ and 800. Inset: the relative difference between the temperature profiles corresponding to $\lambda = 1$ and $\lambda = 1/4$, with $\gamma = 1$ and for $N = 400, 800$ and 1600 (dashed, solid and dotted-dashed lines, respectively).

position along the chain, $y \equiv 2i/N - 1$, that varies in the interval $[-1, 1]$. The data collapse is coherent with the scaling assumed in the continuum approach [7]. The shape of the profile is qualitatively similar to that obtained for fixed BC, although here there are no (square-root) singularities at the boundaries of the chain (see equations (19) and (79) in [7]). Furthermore, we note that the profile itself depends on both γ and λ. Evidence of such a dependence can be appreciated in the inset of figure 4, where the difference $\delta T(y)$ between the profiles corresponding to $\lambda = 1$ and $1/4$ is plotted for three different system sizes. In fact, we see that $\delta T(y)$ does not vanish in the thermodynamic limit. Moreover, the regions around the boundaries are affected by strong finite-size effects. In fact, one expects that $\delta T(-1) = \delta T(1) = 0$, as the temperature necessarily converges, as $N \to \infty$, to that of the attached heat bath.

3.3. Other correlators

In this section we analyse the behaviour of the different correlators (3), along the diagonal $(i = j)$ and for generic values of $x = (i - j)/\sqrt{N}$.[7] We first analyse the case of fixed BC.

At equilibrium, off-diagonal elements of the correlators (3) are zero. In the nonequilibrium steady state we have recently shown that the off-diagonal correlators $\mathbf{v}$ are of $O(1/\sqrt{N})$ [7]. This is confirmed in figure 5(*a*), where we plot the lower diagonal of $\mathbf{v}_{i,i+1}$, corresponding to $\mathbf{v}$ measured at a distance $x = 1/\sqrt{N}$ from the diagonal, that is denoted by $x = 0^+$.

The potential energy profile $\mathbf{y}$ closely reproduces the kinetic energy profile (see also [6]). In order to appreciate its contribution, it is necessary to look at higher order corrections. This can be done by introducing

$$\psi_{i,j} = \mathbf{v}_{i,j} - \omega^2 \mathbf{y}_{i,j} \tag{9}$$

which measures the mismatch between kinetic and potential energy. Figure 5(*b*) shows that along the diagonal (see the lower set of curves), ψ scales as $1/N$ everywhere except perhaps at the boundaries. From a physical point of view, this implies that everywhere in the bulk, the system is locally at equilibrium (with $1/N$ finite-size deviations from the virial equality). The wild behaviour observed near the boundaries suggests the existence of nontrivial boundary

[7] The continuous coordinate x measures the distance of a given correlator from the diagonal. We have used the same notation in [7].

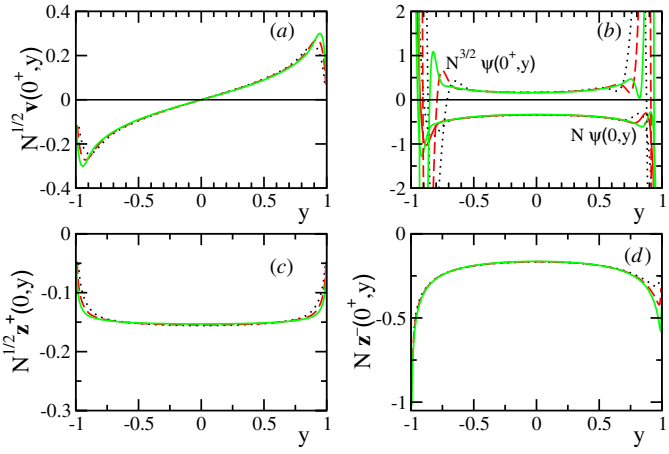

Figure 5. Behaviour of the stationary covariances as a function of the coordinate y for fixed BC and different sizes: (*a*) first lower diagonal of $\mathbf{v}$, (*b*) diagonal (lower curves) and first subdiagonal (upper curves) of ψ, (*c*) diagonal of the symmetric component $\mathbf{z}^+$ and (*d*) first subdiagonal of the antisymmetric component $\mathbf{z}^-$. In all panels, the dotted, dashed and solid lines refer to $N = 200$, 400 and 800 respectively. The physical parameters are $\gamma = 1$ and $\lambda = 1$.

layers. We will discuss this in detail in the next subsection. Analogously to $\mathbf{v}$, ψ exhibits a 'discontinuity' when moving away from the diagonal. Indeed, in the upper set of curves of figure 5(*b*) we show that $\psi(x = 0^+, y)$ is of order $1/N^{3/2}$. It is worthwhile remarking that this scaling holds only for $\lambda = 1$. For $\lambda \neq 1$ we have found that the off-diagonal terms of ψ are of order $1/N$ too. By recalling that here we have selected $\omega = 1$, it is reasonable to conjecture that the faster convergence of ψ observed for $\lambda = 1$ is a manifestation of the thermal impedance matching on the boundary, theoretically predicted for $\lambda = \omega$ (see [8]).

Moreover, as shown in [8], it is convenient to distinguish between symmetric and antisymmetric components of the correlators $\mathbf{z}$ with respect to x:

$$\mathbf{z}^{\pm}_{i,j} = \frac{\mathbf{z}_{i,j} \pm \mathbf{z}_{j,i}}{2} \,. \tag{10}$$

In figure 5(*c*), we plot the symmetric component which corresponds to the leading term of the heat flux. In fact, it scales as $1/\sqrt{N}$. The deviations from a perfectly flat shape reveal again the presence of nontrivial boundary layers. Along the diagonal the antisymmetric component $\mathbf{z}^-$ is zero by construction, while along the first subdiagonal, $\mathbf{z}^-$ scales as $1/N$ (see figure 5(*d*)).

In figure 6 we show the behaviour of the correlators as a function of their distance x from the diagonal. We have found that $\mathbf{z}^-$ and the derivative of $\mathbf{z}^+$ along x are both discontinuous across the diagonal, in agreement with the theoretical analysis in [8]. All the results are independent of λ except for the variable ψ which, for $\lambda \neq 1$, is constant away from the diagonal and of order $1/N$. We would like to remark that this anomaly does not affect the theoretical analysis carried in [7] and [8], as (for fixed BC) ψ does not contribute to the leading behaviour of the temperature profile and of the heat flux.

The very good overlap among the curves obtained for different system sizes confirms the scaling behaviour of the off-diagonal already seen in figure 5. Most important, the observed scaling corroborates the validity of the *ansatz* used in [7] and [8]. Summarizing, for fixed BC and far from the boundary we find the following.

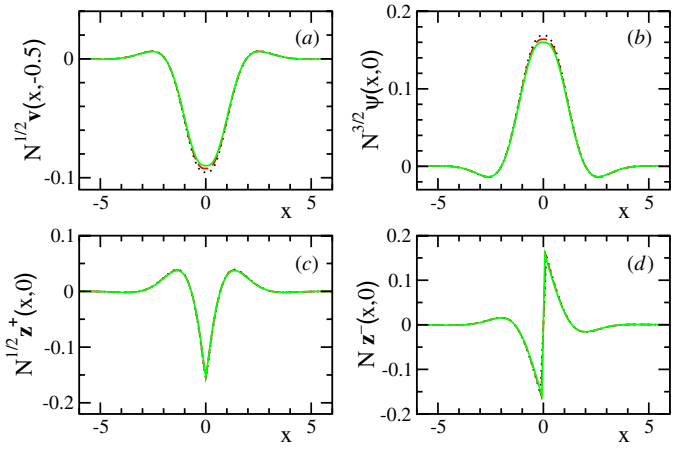

Figure 6. Off-diagonal behaviour of the stationary covariances for fixed BC and the same parameter values and same notations as in the previous figure: (*a*) $\mathbf{v}$ for $y = -0.5$; (*b*) ψ for $y = 0$; (*c*) $\mathbf{z}^{+}$ for $y = 0$ and (*d*) $\mathbf{z}^{-}$ for $y = 0$. The physical parameters are $\gamma = 1$ and $\lambda = 1$. For the sake of clarity, in panels *a* and *b* the diagonal values ($x = 0$) are omitted as they are of lower order.

- Along the diagonal, ψ is $O(1/N)$. Off-diagonal, ψ is $O(1/N^{3/2})$ for $\lambda = \omega$ and $O(1/N)$ otherwise.
- The correlator $\mathbf{v}$ is $O(1)$ along the diagonal and $O(1/\sqrt{N})$ off-diagonal.
- The symmetric correlator $\mathbf{z}^{+}$ is $O(1/\sqrt{N})$ everywhere.
- The antisymmetric correlator $\mathbf{z}^{-}$ is $O(1/N)$.

As a final remark, note that $\mathbf{z}^{+}$ is the only variable that is continuous in x. This implies that the difference $\mathbf{z}^{+}(0^{+}, y) - \mathbf{z}^{+}(0, y)$, that we have denoted by $\delta\mathbf{z}^{+}$ in [8], must necessarily be an order ε higher than its addenda, since its leading contribution is a derivative with respect to x.

We now turn our attention to the free BC. As can be seen in figure 7, the correlators scale with N in the same manner, irrespectively of the boundary conditions. We only note the following qualitative differences: first, with free BC, the convergence at the boundaries is more effective than for fixed BC (compare figure 5(*b*) with figure 7(*c*)). Second, as a function of x, some additional oscillations of $\mathbf{z}$ can be seen only for fixed BC (figures 5(*c*) and 7(*b*)). Third, $\mathbf{z}^{+}$ is larger for free BC, in agreement with the fact that in this case, the heat flux is about two times larger than that for fixed BC.

3.4. Behaviour at the chain edges

The numerical discussion carried out in the previous subsection has revealed the existence of 'boundary layers' in the vicinity of the contact points with the heat baths ($y \approx \pm 1$), where strong deviations from the expected scaling behaviour are clearly visible. Since in [8], we have not attempted a theoretical analysis of the boundary layers, it is at least necessary to clarify their relevance, with reference to the numerical but otherwise exact solutions for the correlators.

The variable that is mostly affected by the presence of such boundary layers is ψ which even changes its scaling behaviour with N. This is shown in figure 8 for the case of fixed BC. In order to emphasize the scaling behaviour at the boundary, we subtract from ψ the

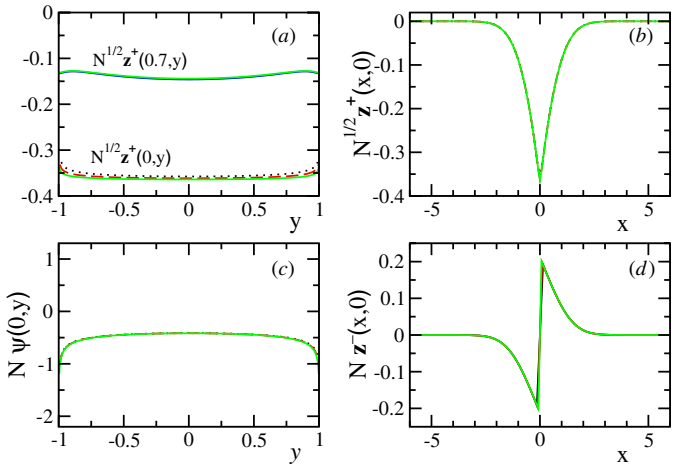

Figure 7. Elements of the stationary covariances for free BC and different sizes: (*a*) $\mathbf{z}^+(x=0,y)$ (lower curves) and at $\mathbf{z}^+(x=0.7,y)$ (upper curves); (*b*) $\mathbf{z}^+(x,y=0)$; (*c*) $\psi(x=0,y)$ and (*d*) $\mathbf{z}^-(x,y=0)$. In all panels, the dotted, dashed and solid lines refer to $N=200,400$ and 800 respectively.

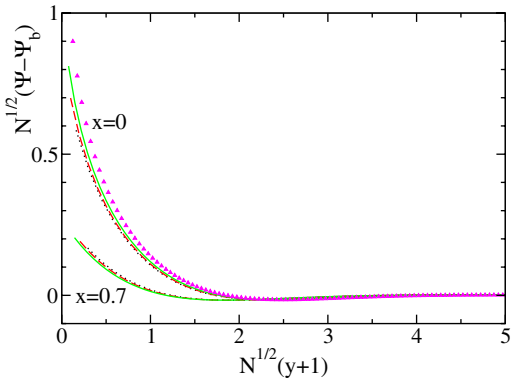

Figure 8. Scaling behaviour of $\psi_{i,j}$ close to the leftmost edge of the chain ($y\approx -1$) for fixed BC and $\gamma=1$. The dotted, dashed and solid lines refer to $N=200,400$ and 800 and $\lambda=1$. The three lower (upper) curves correspond to $x=0.7$ ($x=0$). The triangles correspond to $N=1600$, $\lambda=0.25$ and $x=0$.

$1/N$ term (denoted by ψ_b) in the bulk that we know is constant (see [8]). For fixed BC and $\lambda=1$, $\psi_b=0$, since the leading term is of order $1/N^{3/2}$, while for $\lambda=0.25$, $\psi_b=1/N$ (with a few per cent of uncertainty on the numerical constant.) The data collapse reveals that ψ passes from values of order $1/\sqrt{N}$ to values of higher order over a number of sites of order $\sqrt{N}$.

The existence of a boundary layer manifests itself in the values that different correlators assume at the boundaries (in the vicinity of $y=\pm 1$). At the level of the partial differential equations derived in [8], the BC (either free or fixed) lead to certain mathematical constraints

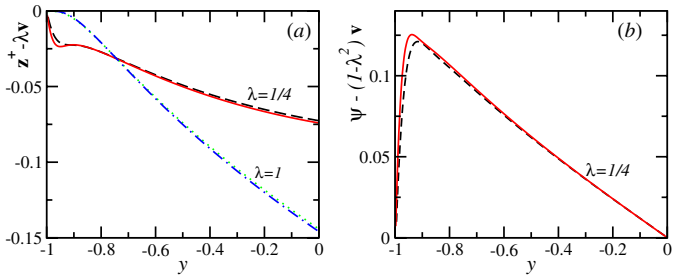

Figure 9. The constraints (11) among the correlators ψ, $\mathbf{z}^+$ and $\mathbf{v}$ are plotted as a function of y and $\omega = \gamma = 1$. The dashed and solid curves correspond to $N = 800$ and 1600, respectively, and $\lambda = 1/4$. The dotted and dotted-dashed curves correspond to $N = 800$ and 1600, respectively, and $\lambda = 1$.

among the correlators that must be satisfied for $y = \pm 1$. For instance, for free BC, we have found analytically that (see equations (64)–(66) of [8])

$$\omega^2 \mathbf{z}^+(x,-1) - \lambda \mathbf{v}(x,-1) = 0, \quad \text{and} \quad (\omega^2 - \lambda^2)\mathbf{v}(x,-1) - \omega^2 \psi(x,-1) = 0. \tag{11}$$

In contrast, for fixed BC we have found that all correlators turn out to be zero at the boundaries. In figure 9 we have plotted the combined variables appearing on the lhs of (11) for ω and γ unity. In panel a, we plot $\mathbf{z}^+ - \lambda \mathbf{v}$ as a function of y for $\lambda = 1$ (dotted and dotted-dashed curves) and $\lambda = 1/4$ (solid and dashed curves). In both cases, the combined variable reaches zero at $y \to -1$, thus confirming the findings in [8]. More importantly, for $\lambda = 1/4$, one can infer that $\mathbf{z}^+ - \lambda \mathbf{v}$ will exhibit a discontinuity at $y = -1$ in the limit $N \to \infty$. This is a direct consequence of the boundary layer which can be further seen in figure 9(b), where we plot $\psi - (1 - \lambda^2)\mathbf{v}$ for $\lambda = 1/4$. Furthermore, we see that the second theoretical constraint (11) is also satisfied. This means that ψ becomes of the same order as $\mathbf{v}$. From a physical point of view this implies that in the boundary layer, i.e. at a short distance from the boundaries (of the order of $\sqrt{N}$), local equilibrium does not hold.

4. Relaxation to the stationary state

Another interesting issue of nonequilibrium phenomena concerns the convergence towards the stationary state, with a particular reference to the time scales. In the context of our stochastic model, this question can be addressed by investigating time-dependent solutions of equations (4). As the evolution is linear, this can be done by determining the whole spectrum of the corresponding linear operator.

For computational purposes it is actually convenient to recast the problem (4) in a more compact way, by a suitable 'unfolding' of the elements of the matrices $\mathbf{y}$, $\mathbf{v}$ and $\mathbf{z}$ in a linear array $\mathcal{X}$. To minimize memory requirements, we take into account the fact that $\mathbf{y}$ and $\mathbf{v}$ are symmetric by construction and we consider only their independent entries. On the other hand, $\mathbf{z}$ is antisymmetric only in the stationary state . Therefore, at all finite times, all its elements must be considered. Altogether, $\mathcal{X}$ is composed of $M = 2N^2 + N$ independent elements and the equations of motion for the correlators can be formally written as

$$\dot{\mathcal{X}} = \mathbb{L}\mathcal{X} + \mathcal{X}_0 \tag{12}$$

where $\mathbb{L}$ is an $M \times M$ matrix and the vector $\mathcal{X}_0$ contains the source terms proportional to λ. The matrix $\mathbb{L}$ is real but not symmetric and therefore, has M complex conjugate eigenvalues

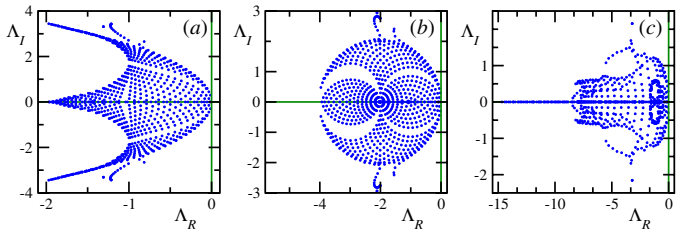

Figure 10. Spectra of the matrix $\mathbb{L}$ for $N = 20$ and $\gamma = 0.5$, 1 and 2 (panel *a*, *b* and *c*, respectively). For the sake of clarity we have used different scales along the vertical and horizontal axes with the exception of panel *b*, where we wish to draw the attention to the nearly circular symmetry.

$\Lambda = \Lambda_R + \mathrm{i}\Lambda_I$. Global stability of the stationary state requires all real parts Λ_R to be nonpositive.

The simplest approach consists in computing the eigenvalue spectra $\{\Lambda_i\}$ of the matrix $\mathbb{L}$ with standard linear algebra algorithms. Their location in the complex plane is illustrated in figure 10 for three different values of γ. First we recall that, to our knowledge, this is the first nontrivial model where all time scales from the microscopic to macroscopic ones can be obtained at once. As expected, the whole spectrum lies on the negative Λ_R semi-plane, confirming that the stationary state is stable. Secondly, we note that the shape of the spectrum changes qualitatively upon varying the collision rate γ. By increasing γ, the real part of the spectrum is shifted towards negative values. This is also not surprising as γ quantifies the strength of the internal stochastic process and thereby of the corresponding relaxation processes. More interesting is the observation that the Λ_R's are distributed over an entire range of scales from O(1) to very small ones. In the perspective of constructing a suitable hydrodynamic description (that is basically the goal of [8]), it is only the latter ones that matter. Unfortunately, we have not found a way to establish a direct connection between slow modes (those characterized by a small $|\Lambda_R|$) and hydrodynamic modes, as this would require determining not only the eigenvalues, but also the eigenvectors. This task is numerically unfeasible, as the dimension of the space increases quadratically with N, and it is not even easy to determine the spectrum, let alone the eigenvectors. In practice, we have been able to determine the entire spectrum only up to $N \sim 80$.

As far as we are concerned with the slowest relaxation processes, we can employ an alternative method akin to that used for the computation of the maximum Lyapunov exponent of a dynamical system. Indeed, for asymptotically long times

$$\mathcal{X}(t) = \mathcal{X}' \mathrm{e}^{\Lambda_1 t}, \tag{13}$$

with some X' which depends on the initial condition (actually it suffices to consider the homogeneous system $\dot{\mathcal{X}} = \mathbb{L}\mathcal{X}$ since $\mathcal{X}_0$ does not affect the relaxation process). In order to estimate Λ_1, we integrated numerically the differential equations (12) starting from random initial conditions with unit Euclidean norm, $\|\mathcal{X}(0)\| = 1$. For the sake of accuracy, we divided the time T_{tot} of the whole run into n consecutive time intervals, each of length τ, so that $T_{\mathrm{tot}}/\tau = n$. At the end of each time interval, we store the corresponding growth rate and renormalize the vector $\mathcal{X}$ to a unit norm. Finally, we determine Λ_1 as the average

$$\Lambda_1 = \frac{1}{n\tau} \sum_{l=1}^{n} \ln \|\mathcal{X}(l\tau)\|. \tag{14}$$

As a result, we have been able to investigate systems of size up to $N = 400$. The numerical results plotted in figure 11(*a*) show that for the considered parameter values, Λ_1 is real and

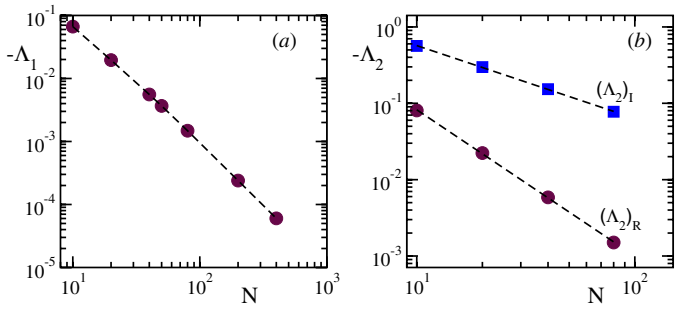

Figure 11. Dependence of the leading eigenvalues on the chain length N, for $\gamma = 1$ and fixed BC. Data are plotted in log–log scales. In panel (*a*), the maximum (real) exponent Λ_1 (circles) is plotted together with a power-law best fit $N^{-1.91}$ (dashed line). In panel (*b*), the real (circles) and imaginary (square) parts of the second eigenvalue Λ_2 are plotted. The dashed lines correspond to the power-law fits $N^{-1.91}$ and $N^{-0.95}$ respectively.

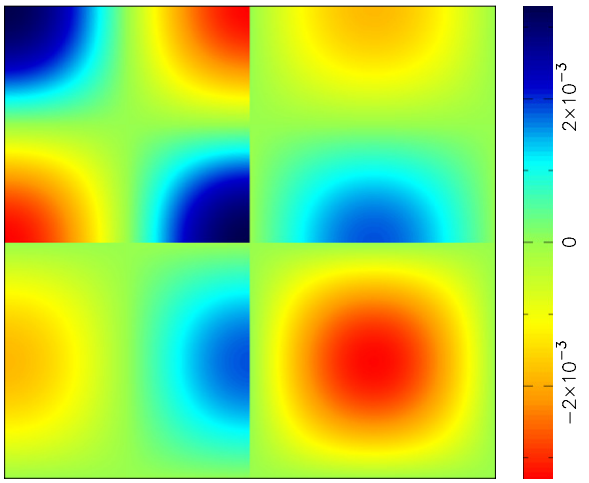

Figure 12. Eigenvector of the linear operator $\mathbb{L}$ corresponding to Λ_1, for $N = 400$ and $\gamma = 1$. Starting from the highest panel on the left and going in clockwise sense, we plot the matrices $\mathbf{y}_{i,j}$, $\mathbf{z}_{i,j}$, $\mathbf{v}_{i,j}$ and $\mathbf{z}^{\dagger}_{i,j}$ respectively.

goes to zero with some power of N. A best fit suggests that $\Lambda_1 \approx N^{-2}$. The same approach allows determining the corresponding (slowest) 'mode' of the linear operator $\mathbb{L}$. In figure 12 we plot the result obtained for $N = 400$. It looks very similar to the Fourier modes that we expect on the basis of the theoretical analysis carried out in [8] and the order of magnitude of the corresponding eigenvalue is in agreement with that analysis.

For $N \leqslant 80$ we have been able to determine the entire spectrum. It turns out that the second and third eigenvalues are complex conjugate. In figure 11(*b*) we plot their real and imaginary parts. The real part scales as $1/N^{1.91}$, a value that, despite the limited amount of data, suggests again an asymptotic $1/N^2$ behaviour. Instead, the imaginary part scales nearly as $1/N$. Since this model is characterized by the presence of sound waves, we expect the

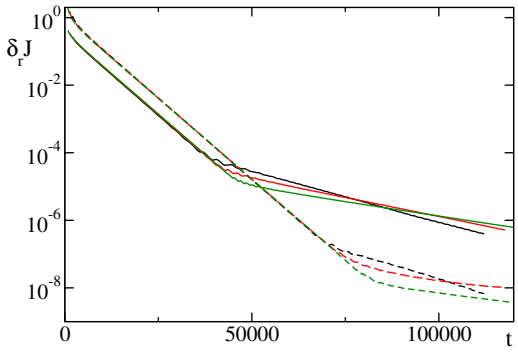

Figure 13. Relaxation of the energy flux to its stationary value for fixed BC, $\gamma = 1$ and $\lambda = 1$. The relative amplitude of the heat flux (see the text for its definition) is plotted versus time for three different sizes ($N = 200, 400, 800$) and for two definitions of the flux. The dashed curves refer to the flux along the first bond of the chain; the solid curves refer to the spatially averaged flux. The time axis refers to the microscopic units for $N = 800$. The time variable for $N = 200$ and $N = 400$ has been scaled by a factor 8.95 and 2.97, respectively, to emphasize the scaling behaviour of the initial exponential regime.

imaginary part of Λ_2 to be connected to the periodicity due to the propagation of such waves. The period T of the oscillations can be written as

$$T = \frac{2\pi}{(\Lambda_2)_I} = \frac{N}{c}, \tag{15}$$

where c is the sound velocity (equal to ω in our arbitrary units), so that

$$c = \frac{N(\Lambda_2)_I}{2\pi}. \tag{16}$$

If we substitute for $(\Lambda_2)_I$ the value found numerically, we obtain $c \simeq 1$, thus confirming our expectations. On the other hand, the $1/N^2$ dependence of the real parts poses problems of consistency with the presence of an anomalous heat transport, as the $1/N^2$ dependence is expected to hold for normal heat conduction. In order to get a better understanding of this, we have investigated the convergence of a specific observable, namely the flux J. More precisely, we have studied the relative deviation of the flux at the time t from its asymptotic value (see equation (20) of [7]). This is shown in figure 13 where, starting from an equilibrium state at the temperature $(T_+ + T_-)/2$ (so that $J(0) = 0$), $\delta_r J(t) = 1 - \frac{J(t)}{J(\infty)}$ is plotted as a function of time. We have considered two different definitions of the instantaneous flux: (i) the energy flux along the first bond (i.e. directly in contact with the heat bath), which corresponds to the dashed curves in figure 13; (ii) the average flux (along the whole chain), which corresponds to the solid curves. Altogether, $\delta_r J(t)$ is a measure of the deviation from the stationary state at time t. In order to compare the curves corresponding to three different sizes ($N = 200$, 400 and 800), the time variable has been suitably scaled. The first part of the curves nicely overlaps along a straight line, which signals an exponential convergence with a rate $\eta(N)$ which, taking into account the temporal rescaling factors, is well reproduced by the law

$$\eta(N) = \frac{\eta_0}{N^{3/2}} + \frac{b}{N^2}. \tag{17}$$

A best fit of the numerical results yields $\eta_0 \approx 4.4$ in good agreement with the second eigenvalue of the operator theoretically derived in [8], that is equal to 4.28 (see the spectrum plotted in figure 1 in [8], which has been obtained by setting all parameters equal to 1). The reason why

the first eigenvalue does not play any role in our numerical study is that the corresponding eigenmode is not excited for our choice of the initial condition that is characterized by exactly the same average temperature as that of the asymptotic stationary state.

The curves reported in figure 13 show that for any finite N there exists a crossover time beyond which a yet slower convergence sets in. By fitting the final slope, one can verify that the time scale of this last part of the convergence process is on the order of N^2, in agreement with the previous spectral analysis. However, it is important to note that this time increases with N and thereby corresponds to increasingly small scales (look at the vertical axis in figure 13). Altogether, this means that the components of the initial state that lie along the slowest components become increasingly small upon increasing the system size N, until they vanish in the thermodynamic limit. One way to understand the unphysical character of these 'super slow' modes is as follows. Any meaningful invariant measure is characterized by a set of correlators, but the converse is not true. Only the covariance matrices $\mathbf{c}$ that are positive semi-definite can correspond to physically meaningful state. For instance, we have verified that a sufficiently large perturbation along the eigenmode depicted in figure 12 leads to unphysical matrices.

5. Discussion and conclusions

The study of heat transport in a chain of N particles with nearest-neighbour coupling and conservative noise allows one to investigate both analytically [7] and numerically many subtle aspects of anomalous transport in one-dimensional systems. Since an analytical solution is available only for fixed BC, the free BC case can be investigated only by means of numerical methods. The comparison between the two cases shows that the physics of heat transport strongly depends on the choice of BC. For instance, as already observed in the FPU-β model [10], the ratio between the heat fluxes measured with free and fixed BC does not converge to 1 in the thermodynamic limit ($N \to \infty$). Moreover, we find that for fixed BC the heat flux and the temperature profile are independent of the coupling strength with the thermal bath, while this does not hold for free BC. Nonetheless, the anomalous scaling of heat conductivity with the system size ($\kappa \sim N^{1/2}$) is found to be independent of the choice of BC. We have also investigated the convergence to the stationary state, both by determining the eigenvalues of the evolution operator of the covariance matrix, and by following the evolution of the average heat flux when starting away from the stationary state. The analysis reveals that over long time scales, the convergence is controlled by a rate $\eta(N)$ which scales as $N^{-3/2}$. This means that if one wishes to extract reliable numerical data by performing direct numerical simulations, e.g. in a lattice of size $N = 50\,000$, it is necessary to evolve the system well above 10^7 time units. It should be kept in mind that similar limitations hold for deterministic nonlinear systems, even though they are, in general, characterized by slightly different exponents [10]. Finally, our analysis of the time-dependent solution has revealed a crossover from a typical fractional diffusion regime to a super slow relaxation. The crossover time is found to increase with the system size, suggesting that the latter regime becomes irrelevant in the thermodynamic limit.

Acknowledgments

We acknowledge Gianpiero Puccioni for his support in the implementation of the numerical codes. This work is partially supported by the the Italian project *Dinamiche cooperative in strutture quasi uni-dimensionali* no 827 within the CNR programme Ricerca spontanea a tema

libero. CM-M acknowledges partial funding from the European Research Council and the Academy of Finland.

References

[1] Bonetto F, Lebowitz J L and Rey-Bellet L 2000 Fourier's law: a challenge to theorists *Mathematical Physics* eds A Fokas, A Grigorian, T Kibble and B Zegarlinski (London: Imp. Coll. Press) pp 128–50
[2] Lepri S, Livi R and Politi A 2003 Universality of anomalous one-dimensional heat conductivity *Phys. Rev.* E **68** 067102
[3] Dhar A 2009 Heat transport in low dimensional systems *Adv. Phys.* **57** 457
[4] Chang C W *et al* 2008 Breakdown of Fourier's law in nanotube thermal conductors *Phys. Rev. Lett.* **101** 075903
[5] Basile G, Bernardin C and Olla S 2006 Momentum conserving model with anomalous thermal conductivity in low dimensional systems *Phys. Rev. Lett.* **96** 204303
[6] Delfini L, Lepri S, Livi R and Politi A 2008 Nonequilibrium invariant measure under heat flow *Phys. Rev. Lett.* **101** 120604
[7] Lepri S, Mejia-Monasterio C and Politi A 2009 A stochastic model of anomalous heat transport: analytical solution of the steady state *J. Phys. A: Math. Theor.* **42** 025001
[8] Lepri S, Mejia-Monasterio C and Politi A 2010 Nonequilibrium dynamics of a stochastic model of anomalous heat transport *J. Phys. A: Math. Theor.* **43** 065002
[9] Lepri S, Livi R and Politi A 2003 Thermal conduction in classical low-dimensional lattices *Phys. Rep.* **377** 1
[10] Delfini L, Lepri S, Livi R and Politi A 2008 Comment on 'Equilibration and universal heat conduction in Fermi-Pasta-Ulam chains' *Phys. Rev. Lett.* **100** 199401